





RESEARCH ARTICLE

Correlation between lactate dehydrogenase/pyruvate dehydrogenase activities ratio and tissue pH in the perfused mouse heart: A potential noninvasive indicator of cardiac pH provided by hyperpolarized magnetic resonance

David Shaul  | Assad Azar | Gal Sapir  | Sivaranjan Uppala |
Atara Nardi-Schreiber  | Ayelet Gamliel | Jacob Sosna | J. Moshe Gomori |
Rachel Katz-Brull 

Department of Radiology, Hadassah Medical Center, Hebrew University of Jerusalem, The Faculty of Medicine, Jerusalem, Israel

Correspondence

Rachel Katz-Brull, PhD, Department of Radiology, Hadassah Medical Center, Hebrew University of Jerusalem, The Faculty of Medicine, 1 Kalman Mann Street, POB 12000, Jerusalem 9112001, Israel.
Email: rkb@hadassah.org.il

Funding information

Horizon 2020 Framework Programme FP7, European Research Council, Grant/Award Number: 338040; Horizon 2020 Framework Programme, Grant/Award Number: 667192; Israel Innovation Authority, Grant/Award Number: 63361; Israel Science Foundation, Grant/Award Number: 1379/18; Israel Ministry of Science and Technology, Grant/Award Number: 3-15892

Cardiovascular diseases account for more than 30% of all deaths worldwide and many could be ameliorated with early diagnosis. Current cardiac imaging modalities can assess blood flow, heart anatomy and mechanical function. However, for early diagnosis and improved treatment, further functional biomarkers are needed. One such functional biomarker could be the myocardium pH. Although tissue pH is already determinable via MR techniques, and has been since the early 1990s, it remains elusive to use practically. The objective of this study was to explore the possibility to evaluate cardiac pH noninvasively, using in-cell enzymatic rates of hyperpolarized [1-¹³C]pyruvate metabolism (ie, moles of product produced per unit time) determined directly in real time using magnetic resonance spectroscopy in a perfused mouse heart model. As a gold standard for tissue pH we used ³¹P spectroscopy and the chemical shift of the inorganic phosphate (Pi) signal. The nonhomogenous pH distribution of the perfused heart was analyzed using a multi-parametric analysis of this signal, thus taking into account the heterogeneous nature of this characteristic. As opposed to the signal ratio of hyperpolarized [¹³C]bicarbonate to [¹³CO₂], which has shown correlation to pH in other studies, we investigated here the ratio of two intracellular enzymatic rates: lactate dehydrogenase (LDH) and pyruvate dehydrogenase (PDH), by way of determining the production rates of [1-¹³C]lactate and [¹³C]bicarbonate, respectively. The enzyme activities determined here are intracellular, while the pH determined using the Pi signal may contain an extracellular component, which could not be ruled out. Nevertheless, we report a strong correlation between the tissue pH and the LDH/PDH activities ratio. This work may pave the way for using the LDH/PDH activities ratio as an indicator of cardiac intracellular pH in vivo, in an MRI examination.

KEYWORDS

biomarkers, hyperpolarized 13C MR, imaging agent, magnetic resonance spectroscopy, metabolic imaging, metabolism

Abbreviations used: ADP, adenosine di-phosphate; ATP, adenosine tri-phosphate; LDH, lactate dehydrogenase; PCr, phosphocreatine; PDH, pyruvate dehydrogenase; Pi, inorganic phosphate.

1 | INTRODUCTION

Cardiovascular diseases account for more than 30% of all deaths worldwide¹ and are a growing economic burden.² Accordingly, it has become increasingly imperative to develop new diagnostic and prognostic techniques that are able to detect and diagnose cardiac pathologies, provide greater information on the vulnerability of the tissue at risk, and better evaluate the effectiveness of treatments.³ Cardiac imaging is a growing medical technology that is continuously being developed to meet this need.⁴ Current cardiac imaging modalities that provide a window to noninvasively assess functional and anatomical cardiovascular properties include echocardiography, computed tomography angiography and cardiovascular magnetic resonance.⁵ Other modalities allow noninvasive probing of metabolic processes, which enables early diagnosis of cardiovascular pathologies.⁵ These include positron emission tomography (PET), single-photon emission computed tomography (SPECT) and magnetic resonance spectroscopy (MRS).⁵ However, PET and SPECT expose patients to ionizing radiation and the low sensitivity of MRS prohibits its widespread clinical use.⁵ In this regard, extensive effort was invested in finding a noninvasive indicator for the pH level of the tissue, as the acid–base balance is disrupted in the early stages of cardiac diseases and conditions such as myocardial ischemia, maladaptive hypertrophy and heart failure.⁶ Disruption of the acid–base balance can lead to severe consequences for the heart. For example, a decrease in cardiac cytosolic pH below a value of ~ 7.2 could be followed by acute contractile depression, distortion of intracellular Ca^{+2} signaling and even electrical arrhythmia.⁶ It has also been shown that a cytosolic pH of ~ 6.9 contributes to reactive oxygen species production in the reperfused ischemic heart, which eventually leads to oxidative stress, cellular dysfunction and death.⁷ Taken together, it appears that an indication of tissue pH could aid in developing early diagnostics and better characterization of such pathologies and could help target better treatment.

Several magnetic resonance (MR) techniques have been developed to evaluate pH *in vivo* noninvasively. ³¹P-MRS can be used to determine pH based on the chemical shift of inorganic phosphate (Pi).^{8,9} However, the low sensitivity associated with this methodology, which dictates very long acquisition times, prohibits its clinical use outside the clinical research realm. Specifically in the heart, the Pi signal is contaminated by ventricular blood constituents such as 2,3-diphosphoglycerate and phosphodiester,¹⁰ thus further limiting utilization of this technology in this context, although these signals can be eliminated using dedicated acquisition techniques.¹¹

MRS of hyperpolarized ¹³C-labeled substrates allows noninvasive visualization of metabolism without the use of ionizing radiation by providing several orders of magnitude increase in the MR signal-to-noise (SNR) ratio of the labeled site.¹² The rat cardiac pH was probed *in vivo* using this technology by measuring the hyperpolarized $\text{H}^{13}\text{CO}_3^-/\text{}^{13}\text{CO}_2$ signal ratio following administration of hyperpolarized $[1\text{-}^{13}\text{C}]\text{pyruvate}$.¹³ This technique is based on the production of hyperpolarized ¹³CO₂ from hyperpolarized $[1\text{-}^{13}\text{C}]\text{pyruvate}$ catalyzed by pyruvate dehydrogenase (PDH)¹⁴ and further conversion to $\text{H}^{13}\text{CO}_3^-$ by carbonic anhydrase (CA). However, this approach has some limitations: (1) ¹³CO₂ freely diffuses across the plasma membrane, therefore both ¹³CO₂ and $\text{H}^{13}\text{CO}_3^-$ are found in the intracellular and extracellular spaces. The actual pH is regulated in each compartment separately, but as the compartments cannot be monitored separately, the derived pH has some uncertainty in this respect; (2) this approach relies on both compounds being at equilibrium, which is catalyzed by the activity of CA. However, because CA activity is reduced in states of acidic intracellular pH, ischemia, and in several cardiomyopathies,^{13,15,16} the utility of this approach will be limited in such circumstances; and (3) the hyperpolarized ¹³CO₂ signal is ~ 10 -fold smaller than that of $[^{13}\text{C}]\text{bicarbonate}$, and both decay rapidly. Therefore, detection of the ¹³CO₂ signal is challenging.¹³

Compared with hyperpolarized $[1\text{-}^{13}\text{C}]\text{pyruvate}$ administration, injecting hyperpolarized $[^{13}\text{C}]\text{bicarbonate}$ improves the SNR of ¹³CO₂, despite the short T₁ of bicarbonate (T₁ = 10 seconds *in vivo*).¹⁷ Although in this way the dependency on PDH activity is eliminated,¹⁷ the uncertainty in intracellular versus extracellular pH, and the dependency on CA activity, remain.¹⁸ Hyperpolarized $[1,5\text{-}^{13}\text{C}_2]\text{zylonic acid}$ has been shown to be a sensitive extracellular pH marker that is independent of enzymatic activity¹⁹ and was found useful *in vivo* in the rat bladder, kidney, and in adenocarcinoma.²⁰ Several other enzymatically independent hyperpolarized pH reporters have also been investigated,^{21–27} but were only tested *in vitro*.

Despite these advances, currently there is no available clinical method to effectively determine pH in the heart noninvasively. Hyperpolarized $[1\text{-}^{13}\text{C}]\text{pyruvate}$ has been previously used to observe rapid metabolic processes, specifically the production of hyperpolarized $[1\text{-}^{13}\text{C}]\text{lactate}$ and $[^{13}\text{C}]\text{bicarbonate}$, in real time in the rat heart *ex vivo*^{13,14,28–37} and *in vivo*,^{36–50} in the pig heart *in vivo*,^{45,51–58} and recently also in the human heart *in vivo*.^{59,60} In these previous studies, metabolic markers of heart failure,⁴⁰ acute infarction,³⁶ cardiac hypertrophy,⁶¹ ischemic heart⁴² and ischemia–reperfusion injury⁴⁹ have been described. An increase in the ratio of the $[1\text{-}^{13}\text{C}]\text{lactate}$ to the $[^{13}\text{C}]\text{bicarbonate}$ signals, and area under the curve of these signals over time, were reported following ischemia–reperfusion injury *in vivo*⁴⁹ and following acute myocardial infarction of the perfused rat heart.³⁶ All of this prior evidence raises the hypothesis that the activities of lactate dehydrogenase (LDH) and PDH may be related to cardiac tissue acidity. Recently, a correlation between the signal ratio of hyperpolarized $[1\text{-}^{13}\text{C}]\text{lactate}$ and $[^{13}\text{C}]\text{bicarbonate}$ to the signal ratio of hyperpolarized $\text{H}^{13}\text{CO}_3^-$ and ¹³CO₂ was found in acute myocardial ischemia–reperfusion injury and necrosis.⁶² This correlation has suggested a connection between the relative activities of LDH and PDH (LDH/PDH activities ratio) and the tissue pH. However, a quantitative evaluation of this correlation has not been described yet. Here, we have quantitatively investigated this possible correlation between the relative LDH and PDH activities and the tissue pH. For the determination of cardiac pH, we have utilized ³¹P spectroscopy and used a multi-parametric

analysis for the pH distribution as manifested by the heterogeneous chemical shift of the Pi signal of the tissue. The relative activities of LDH and PDH were determined by monitoring the production of hyperpolarized $[1-^{13}\text{C}]$ lactate and $[^{13}\text{C}]$ bicarbonate from hyperpolarized $[1-^{13}\text{C}]$ pyruvate using the hyperpolarized product selective saturating-excitations approach.⁶³ This acquisition approach was recently developed to monitor enzyme activity in a model-free manner that enabled determination of absolute enzymatic rates (ie, the number of product moles that were produced per unit of time). We note that hyperpolarized ^{13}C -labeled pyruvate analogs are the only agents that have been tested clinically^{59,60,64–71} and therefore the findings of the current study are likely translational.

Our studies were carried out using the retrograde perfused mouse heart, also known as the Langendorff heart.^{72–74} The isolated perfused rodent heart is an ex vivo preparation that could preserve a stable pH and tissue viability during at least 80 minutes⁷⁵ and could recover following a prolonged ischemic injury.^{76,77} Nevertheless, inadvertent surgical preparation variability may lead to variable viability and pH levels of different perfused hearts. Previous studies have also provided indications for the deterioration of this heart preparation over time,⁷⁴ such as, for example, a reduction of 5%–10% per hour in contractile function.⁷³ Here, we have noted that this heart model may occasionally show inadvertent variable starting viability levels and pH. In addition, we noted a gradual decrease in the tissue energetic status with time and that the intracellular pH is subjected to changes over the course of a few hours, although the perfusion and the oxygen supply were uninterrupted. These observations were in agreement with other studies that showed deterioration of this preparation with time.^{73,74} We have capitalized on this inadvertent property of the ex vivo system to obtain a model system of variable and changing cardiac pH in search of a metabolic signature that could serve as an indicator of cardiac pH.

2 | METHODS

2.1 | Experimental workflow

At the beginning of each experiment, a ^{31}P NMR spectrum of the circulating Krebs–Hensleit (KH) buffer to be used in that experiment was acquired. This spectrum showed the signal of the buffer's Pi during flow, using the same parameters that were used for the ex vivo acquisitions. Then the surgical procedure began, during which the mouse heart underwent aortic retrograde cannulation in vivo before being isolated. The isolated mouse heart was then immediately perfused with oxygenated KH buffer at 37°C using a peristaltic pump at a constant flow rate of 7.5 mL/minute. After visual confirmation of the spontaneous return of the heart beating, the heart was inserted into a 10 mm NMR tube and fixed in the tube such that it would be at the center of the NMR probe. An NMR-compatible temperature sensor was also fixed inside the NMR tube just above the heart and two outflow lines for the perfusion system were inserted as well. Then the tube with the perfused beating heart and all other lines were inserted into the bore of a NMR spectrometer.

^{31}P spectra were acquired for ~1 hour to demonstrate cardiac viability and to determine the cardiac pH. This was followed by injection of hyperpolarized $[1-^{13}\text{C}]$ pyruvate to quantify $[1-^{13}\text{C}]$ lactate and $[^{13}\text{C}]$ bicarbonate production using product selective saturating excitations and ^{13}C NMR spectral acquisitions. Each isolated heart ($n = 9$) was subjected to one to three injections of hyperpolarized $[1-^{13}\text{C}]$ pyruvate (total number of injections = 15). Before and after each hyperpolarized injection, a ^{31}P spectrum was acquired.

2.2 | Chemicals

The OX063 radical (GE Healthcare, UK) was obtained from Oxford Instruments Molecular Biotools (Oxford, UK). $[1-^{13}\text{C}]$ pyruvic acid was purchased from Cambridge Isotope Laboratories (Tewksbury, MA, USA). NaCl, KCl, D-glucose, NaHCO_3 , MgCl_2 , $\text{NaH}_2\text{PO}_4(2\text{H}_2\text{O})$, MgSO_4 , pyruvic acid and CaCl_2 were purchased from Sigma-Aldrich (Rehovot, Israel). Insulin aspart 100 U/mL medical grade solution (Novo Nordisk, Denmark) was purchased from Hadassah Medical Center. Isoflurane was obtained from the Authority for Biological and Biomedical Models of the Hebrew University.

2.3 | Experimental medium

We used a modified version of the KH buffer,⁷⁸ which contained 10 mmol/L glucose, 0.5 mmol/L pyruvate, 118 mmol/L NaCl, 4.7 mmol/L KCl, 1.2 mmol/L CaCl_2 , 1.2 mmol/L MgSO_4 , 25 mmol/L NaHCO_3 , 1.2 mmol/L KH_2PO_4 and 72 U/L insulin, all dissolved in water (90/10 v/v double-distilled $\text{H}_2\text{O}/\text{D}_2\text{O}$). Insulin was added to the perfusion buffer following the work of Kolwicz et al⁷⁸ and in agreement with research which reported that insulin increased contractile function⁷⁹ and the intensity of the hyperpolarized $[^{13}\text{C}]$ bicarbonate signal.⁸⁰ Two hundred mL of this buffer were kept in a water bath at 40°C outside the NMR spectrometer and bubbled with 95%/5% O_2/CO_2 for 1 hour prior to cardiac perfusion and continuously bubbled with this gas mixture throughout the experiment at a flow rate of 4 L/minute. The pH of the buffer was 7.4.

2.4 | Animals

Male HSD:ICR (CD-1) mice ($n = 13$, 39–50 g) were obtained from the Institutional Authority of Biological and Biomedical Models of the Hebrew University. The joint ethics committee (IACUC) of the Hebrew University and Hadassah Medical Center approved the study protocol for animal welfare (MD-19-15,827-1). The Hebrew University is an AAALAC International-accredited institute. Care was taken to minimize pain and discomfort to the animals. Only male mice were used due to a limitation dictating the use of NMR tubes of 10 mm in diameter in our spectrometer. Adult and adolescent rat hearts (male and female) were tested and were found to be too large for use in this confined space. Female mice hearts were too small in terms of the ^{31}P SNR that could be obtained at a reasonable acquisition time. Adult male mice weighing more than 39 g were found to be just large enough to both fit the particular spectrometer set-up in our lab and provide the sufficient SNR needed for quantifying adenosine tri-phosphate (ATP) and the tissue pH.

2.5 | Surgical procedure

Animals were anesthetized with isoflurane using a gas anesthesia system (Somnosuite, Kent Scientific, Torrington, CT, USA) at 3.5% and 340 mL/minute of room air for induction and 2.9% isoflurane for maintaining anesthesia. After obtaining negative pedal pain reflex, the surgery began and the heart was exposed. Aortic cannulation was performed *in vivo*, as previously described.⁷² Briefly, 200 IU heparin were injected into the left ventricle to prevent blood coagulation and 0.1 mL of 0.5 mol/L KCl was injected into the right atrium to achieve cardiac arrest. A loose knot of 3–0 silk suture was then placed around the ascending aorta. Cannulation was performed *in situ* with a 22 G intravenous catheter (Model: 381323, BD Medical, Franklin Lakes, NJ, USA). This was followed by suture tightening. The heart was then disconnected from the surrounding viscera and connected to the perfusion system via the catheter. Upon initiation of perfusion with warm buffer at 7.5 mL/minute, the heart began beating spontaneously. The NMR tube with the beating heart was fixed and inserted into the bore of the spectrometer, ensuring that the heart was at the center of the NMR probe.

2.6 | Perfusion system

The perfusion system was made of medical grade extension tubes and the KH buffer was circulated with a peristaltic pump (Masterflex L/S Economy Variable-Speed Drive model 07554–95, Cole-Parmer, Vernon Hills, IL, USA). Thin polyether ether ketone (PEEK) lines (id. 0.040", Upchurch Scientific, Inc., Oak Harbor, WA, USA) were used for buffer and hyperpolarized agent flow to and from the NMR tube. The magnetic susceptibility of PEEK is similar to water and therefore can be used during NMR spectroscopy recordings. The inflow line was connected to the intravenous catheter with a homemade adapter. The temperature of the KH buffer inside the NMR spectrometer during the perfusion was 37–37.5°C and was measured continuously and simultaneously with the NMR recordings using an NMR-compatible temperature sensor (Osensa, Burnaby, BC, Canada).

2.7 | Tissue wet weight and volume determination

At the end of the experiment, the heart was disconnected from the perfusion system, lightly dried with tissue paper then weighed to determine the tissue wet weight (Table S1). The average weight of the hearts used in the current study was 288.5 ± 50 mg ($n = 13$). The volume of the heart was estimated using a density factor of 1.05 g/cm³ determined previously for the mouse heart.⁸¹

2.8 | DNP spin polarization and dissolution

Spin polarization and fast dissolution were carried out in a dissolution-DNP (dDNP) spin polarization device (HyperSense, Oxford Instruments Molecular Biotools) operating at 3.35 T. A microwave frequency of 94.110 GHz was applied for polarization of the [1- ^{13}C]pyruvic acid formulation at 1.45 to 1.55 K. The formulations consisted of 11.1 to 14.0 mmol/L OX063 radical in the neat acid. The dissolution medium consisted of TRIS-phosphate buffer (4 mL), which contained 11.2 mmol/L NaH₂PO₄, 38.8 mmol/L Na₂HPO₄, 33 mmol/L TRIS and 2 mmol/L HCl. This medium composition was adjusted such that upon addition of 15 mg [1- ^{13}C]pyruvic acid formulation (in the dissolution phase) the pH of the resulting solution will be 7.4. Prior to the administration of medium to the heart, the hyperpolarized medium (4 mL) ejected from the dDNP device was quickly mixed with a well oxygenated solution that was designed to complement the hyperpolarized dissolution medium, such that the injected medium to the heart will have a composition that is as close as possible to the perfusion medium. The final volume of the medium perfusing the heart

during the hyperpolarized injections with 14 and 5 mmol/L hyperpolarized [1-¹³C]pyruvate was 12 and 26 mL, respectively. The final composition of the injected medium (after mixing) contained 4.7 mM KCl, 1.2 mM MgSO₄, 70 mM NaCl, 25 mM NaHCO₃, 1.2 mM KH₂PO₄, 10 mM glucose, 1.2 mM CaCl₂ and 72 U/L insulin. The injection of the resulting hyperpolarized [1-¹³C]pyruvate solution to the isolated heart was carried out using a continuous flow set-up⁸² such that the heart perfusion was not interrupted at any point during the experiment and the hyperpolarized medium was administered at a known rate and duration.

2.9 | NMR spectroscopy

³¹P and ¹³C NMR spectroscopy were performed in a 5.8 T high resolution NMR spectrometer (RS2D, Mundolsheim, France) using a 10 mm broad-band NMR probe. ³¹P spectra of thermal equilibrium phosphate signals were acquired with a nutation angle of 50° and a repetition time of 1.1 seconds. The probe was tuned back and forth from ³¹P to ¹³C during the experiment to support the requirement of the experimental workflow, in which several injections of hyperpolarized media were performed into the same perfused heart (and monitored with ¹³C spectroscopy) and the pH and the energy status were monitored using ³¹P spectroscopy before, in between, and after the injections. Homogeneity optimization (shim) was performed using the water signal on the ¹H channel and using the lock system. The ¹H linewidth of water ranged from 15 to 20 Hz.

2.10 | Hyperpolarized ¹³C spectroscopy

Hyperpolarized ¹³C data were acquired using product selective saturating-excitation pulses⁶³ by applying 2.5 ms cardinal sine (Sinc) pulses. The power for this pulse was calibrated on a sensitivity standard sample containing dioxane (40% p-dioxane in benzene-D₆, Cambridge Isotope Laboratories, MA, USA) before each experiment. The pulse was calibrated to provide maximal signal for the product ([1-¹³C]lactate or [¹³C]bicarbonate) frequency, that is, equivalent to a 90° excitation together with an effectively small excitation of the substrate ([1-¹³C]pyruvate). For these selective pulses, nonsinusoidal behavior was found for off-resonance frequencies (see the supporting information in Adler-Levy et al⁸²). For this reason, intensity ratios rather than flip angles were used in the calculation of enzymatic rates. The selective excitations for [1-¹³C]lactate and [¹³C]bicarbonate were carried out consecutively at 6-second intervals, resulting in a 12-second interval for each metabolite. For [1-¹³C]lactate detection, the selective Sinc pulse was centered at the [1-¹³C]pyruvate hydrate frequency (179.4 ppm), which resulted in a signal intensity ratio (ρ_{lac}) of 0.113 for the C₁ signals of [1-¹³C]pyruvate to [1-¹³C]lactate. For [¹³C]bicarbonate detection, the selective Sinc pulse was centered at 157.7 ppm, which is 214 Hz down-field of the [¹³C]bicarbonate signal (161.1 ppm). This resulted in a signal intensity ratio (ρ_{bic}) of 0.139 for the C₁ signal of [1-¹³C]pyruvate to [¹³C]bicarbonate. The [1-¹³C]lactate and [¹³C]bicarbonate signals were fully sampled and depolarized following the application of the respective hyperpolarized product selective saturating-excitation pulses, as described previously.⁶³

2.11 | Data processing and analysis

2.11.1 | Spectral processing

Spectral processing was performed using MNova (Mestrelab Research, Santiago de Compostela, Spain) and DMFIT.⁸⁴

Multi-parametric pH analysis:

The tissue pH was determined based on the chemical shift of the Pi signal, in reference to the phosphocreatine (PCr) signal, on a ³¹P spectrum that was recorded from the same perfused heart used for hyperpolarized ¹³C metabolic investigation, prior to the hyperpolarized medium injection. Previous studies of the isolated rodent heart showed visible distinction between the extracellular and intracellular Pi signals and demonstrated a range of pH values.^{13,85,86} This suggested heterogeneity of pH within the isolated perfused heart, which was observed in the current study as well. In order to evaluate the tissue pH in the current study, it was first necessary to deconvolve and omit the signal of the KH buffer Pi (Pi_{KH}) from that of the total Pi signal (Pi_t). A ³¹P spectrum of KH buffer showed a single Pi signal (Pi_{KH}). This Pi_{KH} signal was fit to a Lorentzian function using DMFIT.⁸⁴ The volume visible to the NMR probe (V_p, 1.375 mL) contains more KH buffer when the sample tube does not contain the heart. To correct for this filling effect we calculated the attenuated buffer signal (Pi_b) using Equation 1A. This signal was then subtracted from (Pi_t) according to Equation 1B to obtain the Pi signal that arises solely from the perfused heart (Pi_h, Figure 1A).

$$Pi_b = Pi_{KH} \frac{(V_p - V_h)}{V_p} \quad (1A)$$

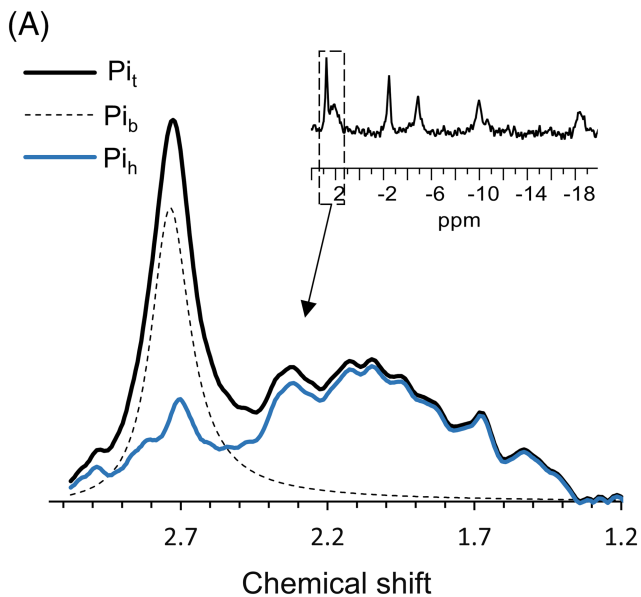
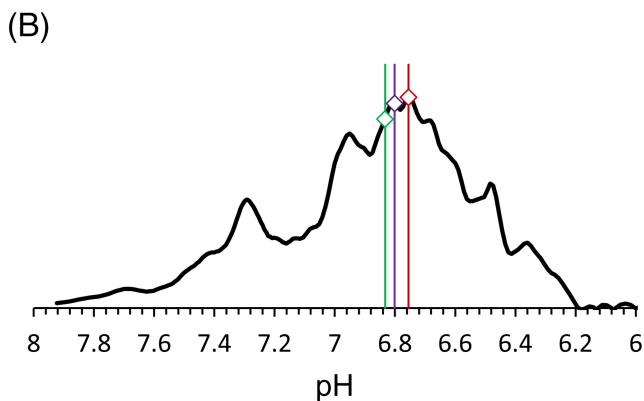


FIGURE 1 The distinction between the Pi signal of the KH buffer and the heart, and conversion from chemical shift to pH axes. A, inset: a typical ^{31}P NMR spectrum acquisition from a mouse heart perfused in the spectrometer with KH buffer. The same spectrum is presented in Figure 2A (first injection). The marked spectral region is shown enlarged. The black curve (Pi_t) is the original spectrum; the dashed curve demonstrates the Pi signal from the buffer only (Pi_b), which was obtained by a fit to a Lorentzian line shape centered at the center of this component of the Pi_t signal and corrected for the amount of KH buffer in the probe following the heart insertion (according to Equation 1A); the blue curve resulted from a subtraction of the Pi_b signal from Pi_t (according to Equation 1B) and represents the Pi signal attributed to the heart (Pi_h). B, conversion of the Pi_h signal to pH distribution and typical multi-parametric analysis of this distribution. The intensities of this distribution were corrected for the nonlinearity between the chemical shift and the pH scales, as previously described.⁸⁷ Vertical lines: green, weighted mean pH (6.83); purple, weighted median pH (6.80); red, global maximum pH (6.75). Skewness, kurtosis, entropy and standard deviation were 0.53, 0.24, 7.81 and 0.29, respectively



$$Pi_h = Pi_t - Pi_b, \quad (1B)$$

where V_h is the volume occupied by the heart, calculated using the heart wet weight (as described above).

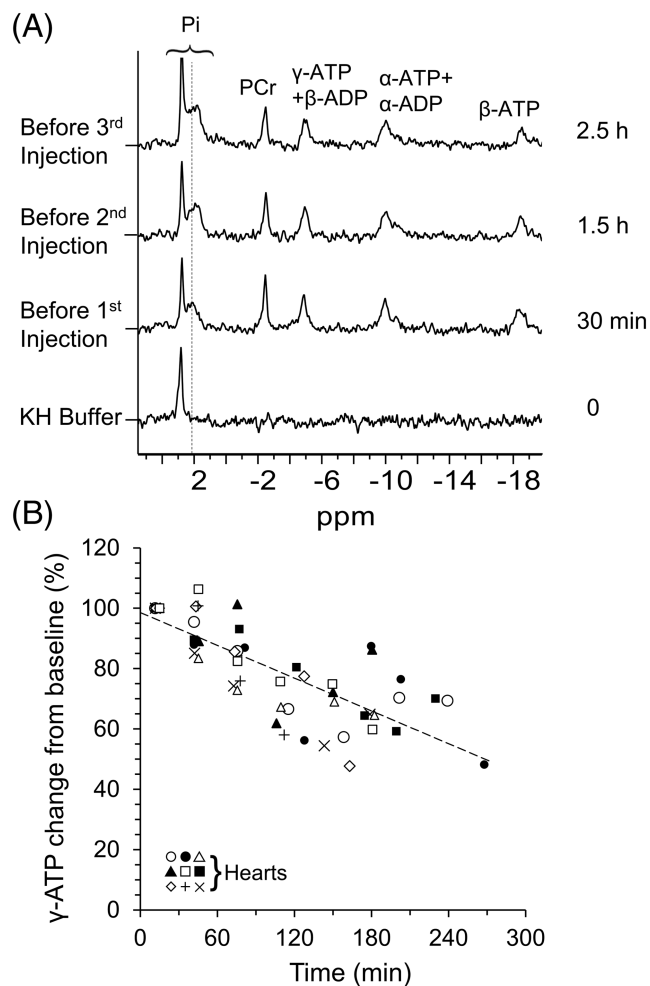
The conversion of the Pi_h signal chemical shift values to pH values was performed with reference to the chemical shift of PCr using Equation 2,⁸⁸

$$pH = pK_a + \log \frac{[\Delta\delta(Pi - PCr) - \delta \text{ free acid}]}{[\delta \text{ free base} - \Delta\delta(Pi - PCr)]}, \quad (2)$$

where $\Delta\delta$ is the chemical shift difference, pK_a is 6.72, δ free base is 5.69 and δ free acid is 3.27, as previously described.⁸⁸ The resulting pH distribution curve was corrected for the nonlinearity between the Pi_h chemical shift scale and the pH scale according to Lutz et al.⁸⁷ A typical pH distribution that resulted from this calculation is presented in Figure 1B.

The tissue pH distributions at various time points during the experiment were analyzed with a multi-parametric approach using seven statistical parameters following the work of Lutz et al.⁸⁷ The parameters used to characterize this heterogeneous pH distribution were: (1) global maximum pH, (2) weighted mean pH, (3) standard deviation of the weighted mean pH, (4) weighted median pH, (5) skewness of the pH plot, (6) kurtosis of the pH plot and (7) statistical entropy.

FIGURE 2 Temporal changes in ^{31}P NMR spectra of isolated mouse hearts. A, typical ^{31}P spectra recorded in one of the experiments. The spectrum at the bottom was acquired from the circulating KH buffer only (30 minutes acquisition). The three upper spectra were acquired from the perfused heart before each hyperpolarized [$1\text{-}^{13}\text{C}$]pyruvate injection. Each spectrum was acquired within 52.5 minutes (a combination of seven spectra acquired during 7.5 minutes each). The time indicated on the right marks the duration between entering the NMR spectrometer and the start of each acquisition. The dashed line marks the approximate center of mass of the tissue Pi signal recorded prior to the first hyperpolarized injection, to assist in qualitative visualization of the tissue acidification over time. B, the temporal changes in ^{31}P NMR $\gamma\text{-ATP}$ signal during 4.5 hours of perfusion of isolated hearts in nine hearts. Each heart is represented by a unique marker. The timescale is referenced to the start of the isolated heart perfusion in the NMR spectrometer (time zero). ^{31}P spectra that were acquired within 30 minutes (a combination of four spectra acquired during 7.5 minutes each) were used for this analysis. The data were normalized to the first point of each experimental day (the baseline). ADP, adenosine di-phosphate; ATP, adenosine tri-phosphate; PCr, phosphocreatine; Pi, inorganic phosphate



2.11.2 | LDH/PDH activities ratio calculation

The LDH/PDH activities ratio was calculated from the rate of production of the hyperpolarized metabolites [$1\text{-}^{13}\text{C}$]lactate and [^{13}C]bicarbonate. As we have used product selective saturating-excitation pulses,⁶³ the hyperpolarized metabolites were fully sampled (and depolarized) by each selective pulse, and only newly synthesized hyperpolarized metabolites were detected on the consequent excitation. To determine the corresponding metabolite production rate, the hyperpolarized [$1\text{-}^{13}\text{C}$]pyruvate signal was used as a reference. During the perfusion with the hyperpolarized medium, the [$1\text{-}^{13}\text{C}$]pyruvate concentration in the NMR tube is first increasing (wash-in), then plateauing (to a maximal concentration of 5 or 14 mmol/L) and then decreasing (wash-out). To be able to determine the time points at which the hyperpolarized [$1\text{-}^{13}\text{C}$]pyruvate concentration was maximal and constant, the [$1\text{-}^{13}\text{C}$]pyruvate signal was corrected for apparent T_1 decay using an apparent T_1 of 53.4 seconds.⁸² This value was previously determined for hyperpolarized [$1\text{-}^{13}\text{C}$]pyruvate in the same spectrometer, at the same pH, temperature and osmolarity, using the same perfusion system, under perfusion arrest, and therefore sums up the effective decay due to T_1 relaxation, RF pulsation, and possible exchange of magnetization with hyperpolarized [$1\text{-}^{13}\text{C}$]pyruvate hydrate. The data points selected for further analysis were those points at which the concentration was within 10% range of the maximal corrected [$1\text{-}^{13}\text{C}$]pyruvate signal. The corresponding data of [$1\text{-}^{13}\text{C}$]lactate and [^{13}C]bicarbonate production for these time points were used for the calculation of metabolite production rates using Equations 3A and 3B. A typical example of such a selection of time points is shown in Figure 3C (highlighted temporal window). For each hyperpolarized injection, the production rates and the activities ratios were calculated within this duration using Equations 3A-3C then averaged.

The following calculation was applied to determine the enzyme activities ratio for each time point:

$$v_{\text{LDH}}(t) = \frac{\rho_{\text{lac}} \times [\text{Pyr}] \times V_{\text{p}}}{\text{TR}} \times \frac{S_{\text{lac}}(t)}{S_{\text{pyr,lac}}(t)} \quad (3A)$$

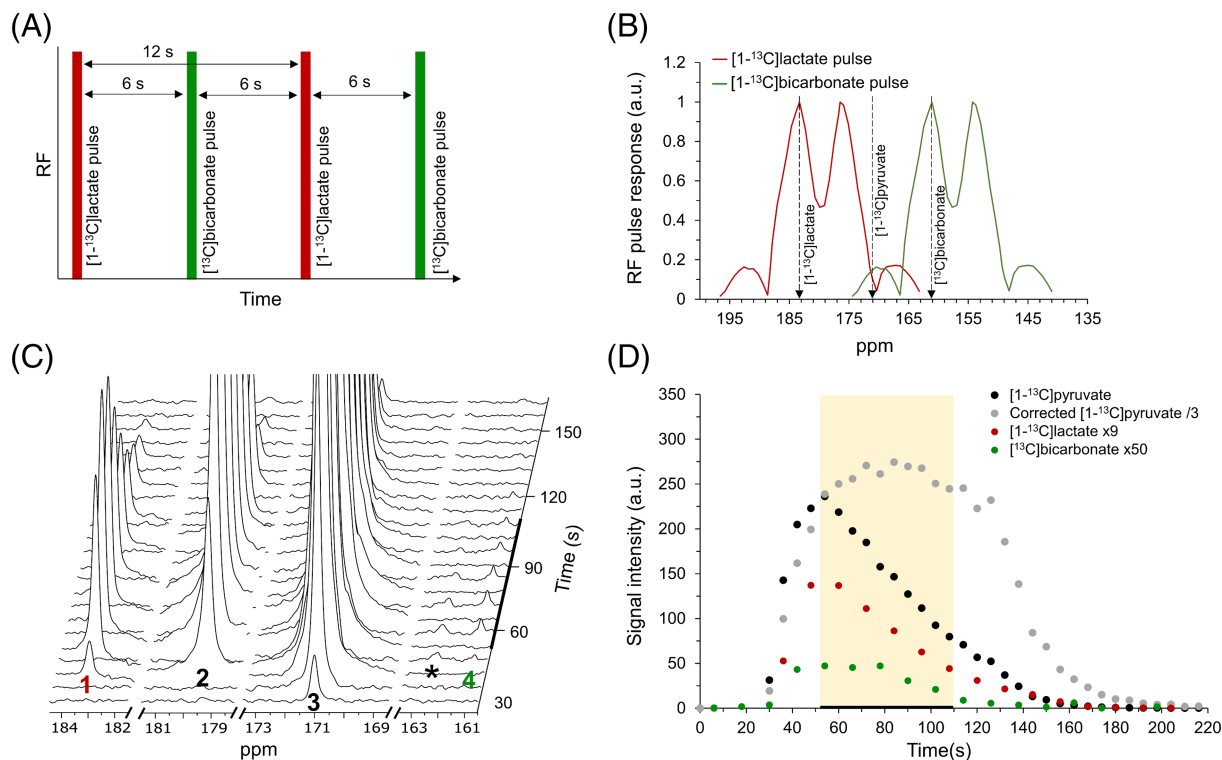


FIGURE 3 Hyperpolarized ^{13}C MRS product selective saturating-excitations acquisition, processing and analysis of $[1-^{13}\text{C}]$ pyruvate metabolism. A, a scheme showing the timing of the excitation RF pulses performed during $[1-^{13}\text{C}]$ pyruvate injection to the perfused heart. The interval between the $[1-^{13}\text{C}]$ lactate and $[^{13}\text{C}]$ bicarbonate selective pulses was 6 seconds, and for each hyperpolarized metabolite, the interval between one excitation to the next was 12 seconds. B, response profiles of the product selective saturating-excitations that were applied for the detection of hyperpolarized $[1-^{13}\text{C}]$ lactate and $[^{13}\text{C}]$ bicarbonate. In this acquisition approach, a Sinc pulse is applied to fully excite (and depolarize) the products $[1-^{13}\text{C}]$ lactate (183.3 ppm) and $[^{13}\text{C}]$ bicarbonate (161.1 ppm). $[1-^{13}\text{C}]$ pyruvate (171 ppm) was excited to a much lower extent on each of the metabolites' excitations, as can be seen in the pulse profile. The response profiles were obtained using excitation of a standard dioxane NMR sensitivity sample (see Methods). C, typical ^{13}C NMR spectra obtained using the hyperpolarized product selective saturating-excitations approach during a typical 14 mmol/L hyperpolarized $[1-^{13}\text{C}]$ pyruvate injection. Signal assignment: 1, $[1-^{13}\text{C}]$ lactate (183.2 ppm); 2, $[1-^{13}\text{C}]$ pyruvate hydrate (179.4 ppm); 3, $[1-^{13}\text{C}]$ pyruvate (171 ppm); 4, $[^{13}\text{C}]$ bicarbonate (161.1 ppm); *, impurity arising from the $[1-^{13}\text{C}]$ pyruvate formulation.⁸³ The thick black line on the time axis marks the time window during which the $[1-^{13}\text{C}]$ pyruvate concentration in the NMR tube was constant as per the analysis in D. D, typical time course of the hyperpolarized signal intensities during the injection shown in C. The $[1-^{13}\text{C}]$ pyruvate integrated intensities (black) were corrected for the effective decay of the signal (due to T_1 relaxation and the applied RF pulses) using an effective decay time constant of 53.4 seconds⁸² (gray). Using this corrected signal time course, a time window (highlighted in yellow, and marked with a thick black line on the time axis) in which the $[1-^{13}\text{C}]$ pyruvate concentration in the NMR tube was constant and maximal was selected for further analysis. For clarity of presentation, the corrected $[1-^{13}\text{C}]$ pyruvate data, the $[1-^{13}\text{C}]$ lactate and the $[^{13}\text{C}]$ bicarbonate data were multiplied by 0.333, 9 and 50, respectively, relative to the $[1-^{13}\text{C}]$ pyruvate signal. a.u., arbitrary units

$$v_{\text{PDH}}(t) = \frac{\rho_{\text{bic}} \times [\text{Pyr}] \times V_p}{\text{TR}} \times \frac{S_{\text{bic}}(t)}{S_{\text{pyr_bic}}(t)} \quad (3\text{B})$$

$$\frac{\text{LDH}}{\text{PDH}} \text{ activities ratio}(t) = \frac{v_{\text{LDH}}(t)}{v_{\text{PDH}}(t)} = \frac{\rho_{\text{lac}} \times S_{\text{lac}}(t) \times S_{\text{pyr_bic}}(t)}{\rho_{\text{bic}} \times S_{\text{bic}}(t) \times S_{\text{pyr_lac}}(t)} \quad (3\text{C})$$

where $v_{\text{LDH}}(t)$ and $v_{\text{PDH}}(t)$ are the production rates of $[1-^{13}\text{C}]$ lactate or $[^{13}\text{C}]$ bicarbonate at each time point, respectively. ρ_{lac} and ρ_{bic} are factors that represent the relative excitation of $[1-^{13}\text{C}]$ pyruvate and the product $[1-^{13}\text{C}]$ lactate and $[^{13}\text{C}]$ bicarbonate, respectively, by the product selective saturating-excitation pulses.⁶³ These factors were determined previously to be 0.113 and 0.139, respectively⁸² (also described above). V_p is the volume detected by the NMR probe (1.375 mL), TR is the duration between consecutive product selective saturating-excitations for each product (12 seconds), $S_{\text{lac}}(t)$ and $S_{\text{bic}}(t)$ are the signals of $[1-^{13}\text{C}]$ lactate and $[^{13}\text{C}]$ bicarbonate at each time point, respectively, and $S_{\text{pyr_lac}}(t)$ and $S_{\text{pyr_bic}}(t)$ are the respective signals of $[1-^{13}\text{C}]$ pyruvate that were acquired using the $[1-^{13}\text{C}]$ lactate and $[^{13}\text{C}]$ bicarbonate excitation pulses, that is,

signals from the same respective spectra (Figure 3B). [Pyr] is the $[1-^{13}\text{C}]$ pyruvate concentration, which was 5 or 14 mmol/L during the plateau phase. We note that in practice, as shown in Equation 3C, the enzyme activities ratio is independent of [Pyr], V_p and TR and that this provides robustness to this indicator.

2.12 | Exponential curve fitting

Curve fitting for the correlation between LDH/PDH activities ratio to the statistical parameters of the pH distribution was performed using Matlab (MathWorks, Natick, MA, USA). All of the experimental data that provided sufficient $[1-^{13}\text{C}]$ lactate and $[^{13}\text{C}]$ bicarbonate SNR to determine both LDH and PDH activities (ie, in the time frame of known $[1-^{13}\text{C}]$ pyruvate concentration) were included in this analysis.

2.13 | Statistical analysis

Multi-parametric analysis of the pH distribution displayed by the ^{31}P spectra was calculated using Microsoft Excel 2016 (Microsoft, Ra'anana, Israel). Curve fitting and calculation of R^2 for goodness of fit and the sum of squares due to error for AIC and BIC scores were performed using Matlab.

3 | RESULTS

3.1 | Changes in cardiac energetics and the tissue pH in the mouse retrograde perfused heart

To test the possible variability in the perfused hearts viability and deterioration, ^{31}P spectra were recorded. Figure 2A displays ^{31}P spectra recorded from a mouse heart perfused with KH buffer and from the buffer alone. The spectrum acquired from the heart shows the signals of α -, β - and γ -ATP, PCr and Pi. The Pi signal is composed of two main components. The component in the higher field (left side of the signal) represents the Pi signal that is mostly due to the KH buffer at a pH of ~ 7.4 . The broader and less homogeneous component in the lower field (right side of the signal) shows the Pi signal, which is in a more acidic environment. The latter component arises from the cardiac tissue (as confirmed by performing similar experiments in a Pi-free KH buffer, [supporting information S1]). It can be appreciated in Figure 2A that the tissue component chemical shift is changing with time, in this case suggesting acidification of the tissue, as previously reported in the rat heart.^{88,89} As regards ATP, overall, we observed a reduction of 10.8% per hour in the intensity of the γ -ATP signal in the isolated hearts investigated here ($n = 9$, $R^2 = 0.61$; linear fit shown in Figure 2B). As the ATP signal reports on myocardial energetic status and viability,⁹⁰ a gradual reduction in its content suggests gradual tissue deterioration.

Next, we investigated the pH status of the same hearts over time using a multi-parametric analysis of the tissue Pi signal (Figure 1). The pH of the isolated rodent heart was previously reported to be 7.1–7.2, and as low as 6.5 during myocardial ischemia.⁶ In these reports, the pH was derived from the use of a radioactive tracer⁹¹ and ^{31}P NMR spectroscopy.⁹² Such pH determinations are likely equivalent to the weighted mean pH determined in our study. In the current study, the weighted mean pH values ranged from 6.64 to 7.26 (Table S1). Although the ATP content showed a common trend of decrease with time (Figure 2B), the tissue acidity was not as consistent. Spectra recorded prior to each hyperpolarized injection showed shifts to acidic pH values but also a return to normal levels from one injection to another, without any clear pattern. Although unintended, the changes in tissue acidity from one heart to another and within the same heart from one point in time to another provided a model system for variable cardiac acidity within the pH range that is clinically relevant.

3.2 | Measurement of the LDH/PDH activities ratio

Due to the use of the hyperpolarized product selective saturating-excitations acquisition approach,⁶³ we were able to perform absolute quantification of the LDH/PDH enzyme activities ratio on each injection. Figure 3 summarizes the acquisition and processing steps that enabled these enzymatic activities ratio determinations.

Table S1 summarizes the LDH/PDH activities ratios measured on all hyperpolarized $[1-^{13}\text{C}]$ pyruvate injections in all of the hearts investigated here, and the multi-parametric pH characteristics that were calculated from ^{31}P NMR spectra acquired 52 minutes prior to each injection. An exponential model was found to describe the correlations between the LDH/PDH activities ratio and four pH characteristics (supporting information Note S2 and Table S2). These characteristics were weighted mean pH (Figure 4A), weighted median pH (Figure 4B), global maximum pH (Figure 4C) and skewness of the pH plot (Figure 4D). The LDH/PDH activities ratio inversely correlated to both the weighted mean pH and the

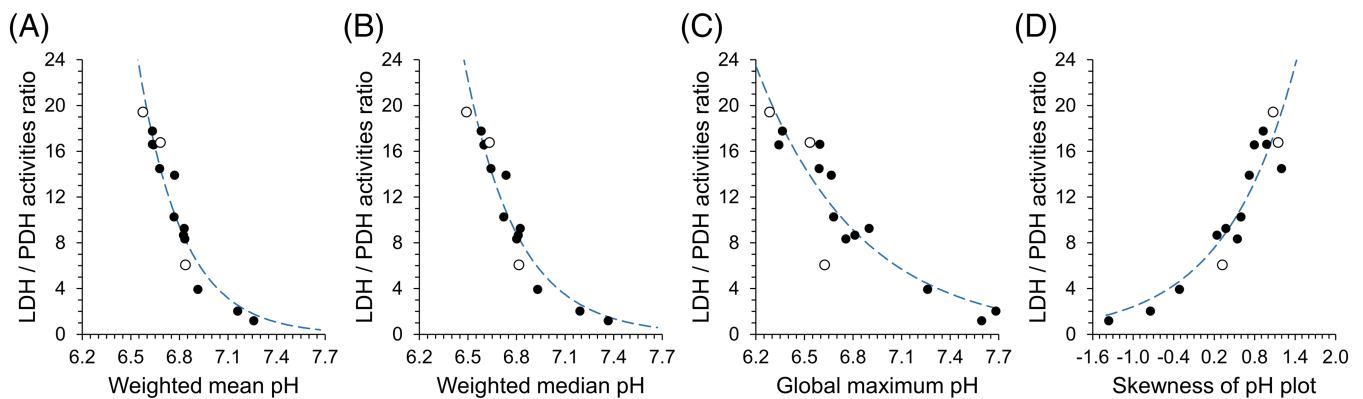


FIGURE 4 The correlation between the LDH/PDH activities ratio and cardiac pH characteristics. Each point represents a single measurement, as described in Table S1. Full circles, injections with 14 mmol/L hyperpolarized [$1\text{-}^{13}\text{C}$]pyruvate (obtained from injections to six hearts); open circles, injections with 5 mmol/L hyperpolarized [$1\text{-}^{13}\text{C}$]pyruvate (obtained from injections to three hearts). Further information on the individual data points is provided in Table S1. A, correlation to the weighted mean pH. The experimental curve was fitted to $y = 5.49 \cdot 10^{11} \cdot e^{-3.65 \cdot x}$ ($R^2 = 0.95$). B, correlation to the weighted median pH. The experimental curve was fitted to $y = 1.2 \cdot 10^{10} \cdot e^{-3.1 \cdot x}$ ($R^2 = 0.94$). C, correlation to the global maximum pH. The experimental curve was fitted to $y = 4 \cdot 10^5 \cdot e^{-1.6 \cdot x}$ ($R^2 = 0.84$). D, correlation to the skewness of the pH plot. The experimental curve was fitted to $y = 6.3 \cdot e^{0.95 \cdot x}$ ($R^2 = 0.86$). y , LDH/PDH activities ratio; x , the relevant statistical characteristic of the pH distribution

weighted median pH with R^2 values of 0.95 and 0.94, respectively. This activities ratio was also inversely correlated to the global maximum pH (Figure 4C) with an R^2 of 0.84, which was lower compared with the R^2 values of the weighted mean pH and weighted median pH. This may be expected as the former two characteristics better represent the entire pH distribution, from which the enzyme activities ratio is derived. As regards the skewness of the pH distribution, a correlation with an R^2 of 0.86 was found. We note that a positively skewed distribution implies that most of the data are located in the right-hand side of the tissue Pi signal (ie, an overall lower pH). Therefore, this correlation to the skewness of the tissue pH distribution is in line with the other three correlations found here. Standard deviation of weighted mean pH, kurtosis and entropy of the pH profile were investigated as well but were not found to correlate with the LDH/PDH activities ratio.

4 | DISCUSSION

In this study, we observed a broad range of tissue pH and enzyme activity ratios. We ascribe these observations to either regional or global variability in cardiac viability. This variability may be caused by two main factors: (1) the delicate surgical procedure in the mouse heart, which involves aortic retrograde cannulation, could damage the heart viability regionally or globally, and therefore the initial condition of each heart may be different; and (2) the perfused heart tissue is heterogeneous with regions of variable perfusion levels, which could vary and change in the course of the experimental day. In agreement, perfusion of the heart with KH buffer was previously reported to be accompanied by tissue deterioration over time.^{73,74} Here, this was demonstrated by a reduction of 10.8% per hour in the γ -ATP signal (Figure 2B).

The wide variety of tissue pH and enzymatic activity ratio that were observed here are likely due to this tissue heterogeneity, which enabled us to sample many points along the tissue pH spectrum. In terms of a potential translation of this study into an in vivo study and possibly to the clinic, it is likely that each imaging voxel in the heart would be heterogeneous as well. Therefore, the correlation between weighted and median pH and the LDH/PDH ratio could be relevant to the in vivo scenario such that this ratio could be an indicator of cardiac pH. It has yet to be shown that the ratio of hyperpolarized $\text{H}^{13}\text{CO}_3^- / ^{13}\text{CO}_2$ correlates with heterogeneous cardiac pH.

The ^{31}P spectra from the perfused heart revealed a nonhomogeneous distribution of the tissue Pi (Pi_i) chemical shift, which suggested a nonhomogeneous distribution of pH in the cardiac tissue. Such a nonhomogeneous distribution was previously described by Lutz et al⁸⁷ in xenograft tumors and was therefore analyzed using a multi-parametric approach. Here, we have used the tools described by Lutz et al⁸⁷ to perform a multi-parametric analysis of the cardiac tissue pH in the perfused mouse heart. To the best of our knowledge, this is the first time that this approach has been implemented in the isolated heart. The Pi_i signal was assumed to predominantly report on the intracellular pH, as the extracellular space is continuously washed by KH buffer, which is at a pH of 7.4 and therefore resonates in a higher field. This assumption was supported in experiments performed with Pi-free KH buffer (supporting information S1).

Both LDH and PDH are intracellular enzymes. While LDH is also present extracellularly in the living animal, in the isolated perfused heart its extracellular activity likely cannot be recorded due to wash out of all metabolites by the perfusing buffer. The hyperpolarized product selective saturating-excitations approach applied here^{63,82} enabled us to determine enzymatic activity in a manner that is independent of variations in T_1 of

the metabolites and the reaction reversibility. By quantifying the ratio of these intracellular activities we provide a robust indicator that is independent of the tissue volume or the amount of cells performing metabolism (Methods), suggesting an indicator that would be independent of voxel size and heterogeneity, if translated to in vivo studies.

As regards the [1-¹³C]pyruvate concentration used here, first, we exposed the isolated hearts to 14 mmol/L hyperpolarized [1-¹³C]pyruvate. We note that this concentration is more than 100-fold higher than the physiological concentration of pyruvate (~0.12 mM).³¹ In addition, in a previous study, we showed that [1-¹³C]pyruvate formulation may contain several impurities that could be toxic to the living cell.⁸³ A previous study showed that increasing the concentration of a 1 mL injection of hyperpolarized [1-¹³C]pyruvate in vivo from 20 to 80 mmol/L led to increased activity of both LDH and PDH, but LDH activity increased by more than that of PDH.⁹³ To convert these injection concentrations to blood concentrations we used the work of Lee and Blaufox,⁹⁴ according to which the blood volume of a 300 g rat is estimated to be 18.8 mL. This resulted in blood concentrations of ~0.92 to 3.7 mmol/L. Schroeder et al.¹³ infused 80 μmol of hyperpolarized [1-¹³C]pyruvate to ~300 g rats in vivo. According to the same conversion, the blood concentration of hyperpolarized [1-¹³C]pyruvate in that study was ~4.3 mmol/L. In perfused heart studies, the hyperpolarized [1-¹³C]pyruvate concentrations ranged from 2 to 3.3 mmol/L.^{13,14,29–36} Altogether, since the injected dose of 14 mmol/L was relatively high compared with prior studies, we wished to test whether this high concentration affects the correlation between LDH/PDH and pH. To this end, we conducted similar experiments, in which the hyperpolarized [1-¹³C]pyruvate concentration was reduced to 5 mmol/L, which is similar to the concentration used by Schroeder et al.¹³ We found that the LDH/PDH activities ratio in the isolated hearts exposed to 14 or 5 mmol/L of hyperpolarized [1-¹³C]pyruvate correlated to pH in the same way (Figure 4). This verified that the results of this ratio-metric approach (LDH/PDH activities ratio) were independent of substrate concentration (in this concentration range). However, we note that the reduction of the hyperpolarized [1-¹³C]pyruvate concentration to 5 mmol/L led to lower SNR of both hyperpolarized products and resulted in an inability to detect the hyperpolarized [¹³C]bicarbonate signal on some of the injections. As a consequence, we report here only on the LDH/PDH activities ratio in the first injection to each heart that was exposed to the 5 mmol/L concentration.

We found that the LDH/PDH activities ratio correlated to the four statistical parameters that characterized the cardiac tissue pH. These were the weighted mean pH, weighted median pH, global maximum pH and the skewness of the pH curve. This result strongly suggested that this enzyme activities ratio is in correlation to the cardiac tissue pH and may serve as an indicator for this parameter. In the absence of an endogenous cardiac pH marker in vivo (as ³¹P is not useful for pH determination in the heart due to blood phosphate constituents¹⁰), such an indicator, which is possible to obtain via injection of an agent that is already regulatory approved, is of key importance.

We note that the LDH/PDH activities ratio was in a better correlation to the statistical parameters that represent the entire pH distribution (weighted mean pH, weighted median pH and skewness of the pH curve) than to the global maximum pH that mostly describes a dominant pH value. Therefore, we believe this indicator could be useful for characterizing cardiac tissue in vivo where each voxel could contain a heterogeneous pH distribution. We note that although the data were best fit to an exponential equation, the underlying mechanisms for this correlation are as of yet unknown. One possible explanation for the exponential relationship could be that the LDH/PDH activities ratio is affected by the hydronium ion concentration in the cell. Indeed, when the data were processed with respect to the hydronium ion concentration of each pH value, a linear correlation was observed.

Our findings are in line with previous knowledge about the connection between pyruvate metabolism and tissue stress such as hypoxia, ischemia and ischemia–reperfusion injury, in which lactate production has been reported to increase while bicarbonate production decreased.^{35,36,49,95,96} Under the same stressors, the acid–base balance is also known to be affected and the tissue generally becomes acidic.^{6,95,96} These previous results may explain the correlation observed here between the LDH/PDH activities ratio and the acidity of the tissue.

Recently, Moon et al.⁶² found a linear correlation between the [1-¹³C]lactate/[¹³C]bicarbonate signal ratio and the pH in myocardial ischemia–reperfusion injury and necrosis in the rat heart. This study was performed in vivo and the pH was measured using the ratio of the hyperpolarized signals of H¹³CO₃⁻ and ¹³CO₂. Because we have determined the absolute ratio of enzyme activities as opposed to hyperpolarized signal ratio on one hand, and tissue pH using the chemical shift of the Pi signal as opposed to the hyperpolarized H¹³CO₃⁻/¹³CO₂ signal ratio on the other, our results cannot be directly compared with those of Moon et al.⁶² The in vivo observation made by Moon et al.⁶² of a similar correlation to the one observed here is encouraging. However, we note several advantages of the current set-up in terms of understanding and validating this correlation: (1) the pH measurement performed here using the chemical shift of the Pi signal is not affected by cellular processes, as opposed to the hyperpolarized H¹³CO₃⁻/¹³CO₂ ratio, which may be affected by the activities of CA, bicarbonate transport and CO₂ diffusion. The need to verify this correlation with ³¹P spectroscopy was also stressed by Moon et al.⁶²; (2) the pH distribution was analyzed here using a multi-parametric approach, therefore, our correlation reliably reflects tissue heterogeneity, which may be less manifested in the signal ratio of hyperpolarized H¹³CO₃⁻/¹³CO₂; (3) here we quantified the relative enzyme activities of LDH and PDH using the product selective saturating–excitations approach.⁶³ This determination is robust and immune to variations in T₁ and excitation profiles and is likely reproducible across labs more than area under the curve analysis, which is dependent on the specific acquisition conditions and set-up in each lab; and (4), in the isolated heart preparation, the metabolic activity is solely from the cardiac tissue and is not affected by wash-in of hyperpolarized metabolites from other organs, as previously demonstrated.⁵⁰

As regards the possible role of ischemia in current studies, although not determined here directly, it is possible that in the isolated hearts studied here, ischemia accompanied (or led to) tissue acidity. In a state of cardiac ischemia, the intracellular pH is decreasing and could reach a value

of 6.5.^{6,97} This acidification has been reported to be mainly due to lactate accumulation,^{6,97} which has a pKa of 3.78.⁹⁸ Other studies in the ischemic rat brain suggested a direct connection between the tissue lactate and pH, based on lactate capability to lower the tissue pH.^{99,100} In the ischemic heart, PDH activity is inhibited, and subsequently bicarbonate production is reduced. This process is attributed largely to elevated levels of NADH, which is a competitive inhibitor of PDH.⁹⁶ This state is also followed by simultaneous increase in the pool of lactate^{95,96} due to reduced levels of NAD⁺. These trends were also observed in a study on the ischemic isolated heart that monitored the metabolism of hyperpolarized [1-¹³C]pyruvate and found that the ratio of [1-¹³C]lactate/[¹³C]bicarbonate signals correlated with the ischemic condition.³⁵ It is possible that the perfused hearts studied here experienced various levels of global or local ischemia due to blockage of blood vessels. We note that this was not an experimentally intended ischemia and the perfusion buffer was constantly saturated with 95%/5% O₂/CO₂. However, as this is a possible process in the perfused heart preparation, it may provide an explanation for the correlation between the LDH/PDH activities ratio and the cardiac pH.

Another explanation for our observation could be driven by the reduction in the pH itself. It has been previously shown that in states of reduced myocardial pH in the range of 6.9 < pH < 7.4, LDH activity is increased in the isolated rat heart.¹⁰¹ PDH activity has been shown to be lowered upon reduction in tissue pH in the range of 6.8 < pH < 8.6.^{102,103} In addition, CA activity is reduced in the pH range of 5.5 < pH < 8.0,¹⁵ and the HCO₃⁻/CO₂ equilibrium is pH dependent.¹³ Therefore, the effect of pH on these enzymes activities may also provide an explanation for the mechanism underlying the correlation between the LDH/PDH activities ratio and the tissue pH.

4.1 | Limitations

We demonstrate a correlation between the LDH/PDH activities ratio and global aspects of tissue pH in the isolated perfused mouse heart. However, further application of this correlation is not straightforward, and further investigation is required: (1) a direct connection between pH and LDH/PDH activities ratio is still unclear, because both of these parameters are affected similarly from the tissue deterioration process that the isolated heart is experiencing. It is important to address the nature of this connection and investigate possible situations in which this ratio and cardiac tissue pH are not correlated; and (2) we found correlation for a specific pH range that was present in our study; however, it is still not known whether pH values that extend this range also correlate to the LDH/PDH activities ratio, especially more alkaline pH values.

4.2 | Significance and future plans

Many pathologies and various cardiovascular diseases disrupt the acid–base balance.^{6,8} Moreover, an uncompensated decrease in cardiac cytosolic pH could be followed by acute consequences.⁶ Early diagnosis and better characterization of such pathologies could help target better treatment. For this reason, pH imaging is a major goal for cardiac research. Currently there is no available clinical method to effectively determine pH noninvasively in the heart. Thus, steps towards this goal could have a significant impact. We suggest the LDH/PDH activities ratio as an indicator of cardiac pH that could be assessed without absolute measurement of polarization or metabolite concentrations using a hyperpolarized [1-¹³C] pyruvate injection that is characterized with long T₁ in vivo (~40 seconds)¹⁰⁴ and has already been tested in humans.^{59,60,64–71} In addition to the metabolic routes that have already been visualized following hyperpolarized [1-¹³C]pyruvate administration in multiple tissue types, and qualitative assessment thereof in multiple conditions and pathologies, we offer an acquisition and analysis approach that yields a potential noninvasive indicator of cardiac pH. In future we intend to investigate the mechanism underlying this correlation. To this end we intend to induce intracellular acidification and explore the effects on LDH and PDH activities. In addition, the effects of hypoxia induced by lowering the oxygen concentration in the perfusion medium will also be investigated.

5 | SUMMARY

We have demonstrated an exponential correlation between cardiac pH and the LDH/PDH activities ratio. Our findings suggest a path to noninvasive assessment of cardiac pH changes using major enzyme activities that are determined by the in-cell production rate of hyperpolarized [1-¹³C] pyruvate metabolites in real time using the product selective saturating–excitations approach.

ACKNOWLEDGEMENTS

We thank Dr. Talia Harris for assistance with selective pulses applications. This project has received funding from the European Research Council (ERC) under grant agreement no. 338040, the European Union's Horizon 2020 research and innovation program under grant agreement no. 667192, the Israel Innovation Authority, KAMIN Incentive program, grant agreement no. 63361, the Israel Science Foundation under grant agreement no. 1379/18, and the Jabotinsky Scholarship of the Israeli Ministry of Science and Technology for Applied and Engineering Sciences for Direct PhD Students no. 3–15892 for D.S.

ORCID

David Shaul  <https://orcid.org/0000-0002-6125-1984>

Gal Sapir  <https://orcid.org/0000-0001-6267-5933>

Atara Nardi-Schreiber  <https://orcid.org/0000-0001-6321-1233>

Rachel Katz-Brull  <https://orcid.org/0000-0003-4850-1616>

REFERENCES

1. WHO. Cardiovascular disease. 2016; http://www.who.int/cardiovascular_diseases/world-heart-day/en/. Accessed 23 January 2020.
2. Heidenreich PA, Albert NM, Allen LA, et al. Forecasting the impact of heart failure in the united states a policy statement from the american heart association. *Circ-Heart Fail*. 2013;6(3):606-619.
3. Handley MG, Medina RA, Nagel E, Blower PJ, Southworth R. PET imaging of cardiac hypoxia: Opportunities and challenges. *J Mol Cell Cardiol*. 2011; 51(5):640-650.
4. Fraser AG, Buser PT, Bax JJ, et al. The future of cardiovascular imaging and non-invasive diagnosis: A joint statement from the European Association of Echocardiography, the working groups on cardiovascular magnetic resonance, computers in cardiology, and nuclear cardiology of the European Society of Cardiology, the European Association of Nuclear Medicine and the Association for European Paediatric Cardiology. *Eur J Echocardiogr*. 2006;7(4):268-273.
5. Di Carli MF, Geva T, Davidoff R. The future of cardiovascular imaging. *Circulation*. 2016;133(25):2640-2661.
6. Vaughan-Jones RD, Spitzer KW, Swietach P. Intracellular pH regulation in heart. *J Mol Cell Cardiol*. 2009;46(3):318-331.
7. Lindsay DP, Camara AKS, Stowe DF, Lubbe R, Aldakkak M. Differential effects of buffer pH on Ca²⁺-induced ROS emission with inhibited mitochondrial complexes I and III. *Front Physiol*. 2015;6:58.
8. Gillies RJ, Raghunand N, Garcia-Martin ML, Gatenby RA. pH imaging. *IEEE Eng Med Biol Mag*. 2004;23(5):57-64.
9. Moon RB, Richards JH. Determination of intracellular pH by ³¹P magnetic resonance. *J Biol Chem*. 1973;248(20):7276-7278.
10. Brindle KM, Rajagopalan B, Williams DS, et al. ³¹P NMR measurements of myocardial pH in vivo. *Biochem Biophys Res Comm*. 1988;151(1):70-77.
11. Blamire AM, Rajagopalan B, Radda GK. Measurement of myocardial pH by saturation transfer in man. *Magn Reson Med*. 1999;41(1):198-203.
12. Ardenkjaer-Larsen JH, Fridlund B, Gram A, et al. Increase in signal-to-noise ratio of > 10,000 times in liquid-state NMR. *Proc Natl Acad Sci U S A*. 2003;100(18):10158-10163.
13. Schroeder MA, Swietach P, Atherton HJ, et al. Measuring intracellular pH in the heart using hyperpolarized carbon dioxide and bicarbonate: a ¹³C and ³¹P magnetic resonance spectroscopy study. *Cardiovasc Res*. 2010;86(1):82-91.
14. Merritt ME, Harrison C, Storey C, Jeffrey FM, Sherry AD, Malloy CR. Hyperpolarized C-13 allows a direct measure of flux through a single enzyme-catalyzed step by NMR. *Proc Natl Acad Sci U S A*. 2007;104(50):19773-19777.
15. Kernohan JC. pH-activity curve of bovine carbonic anhydrase and its relationship to inhibition of enzyme by anions. *Biochim Biophys Acta*. 1965;96(2):304-317.
16. Alvarez BV, Johnson DE, Sowah D, et al. Carbonic anhydrase inhibition prevents and reverts cardiomyocyte hypertrophy. *J Physiol*. 2007;579(Pt 1): 127-145.
17. Scholz DJ, Janich MA, Kollisch U, et al. Quantified pH imaging with hyperpolarized ¹³C-bicarbonate. *Magn Reson Med*. 2015;73(6):2274-2282.
18. Korenchan DE, Gordon JW, Subramaniam S, et al. Using bidirectional chemical exchange for improved hyperpolarized [¹³C]bicarbonate pH imaging. *Magn Reson Med*. 2019;82(3):959-972.
19. Hundshammer C, Düwel S, Köcher SS, et al. Deuteration of hyperpolarized ¹³C-labeled zymonic acid enables sensitivity-enhanced dynamic MRI of pH. *Chem Phys Chem*. 2017;18(18):2422-2425.
20. Duwel S, Hundshammer C, Gersch M, et al. Imaging of pH in vivo using hyperpolarized ¹³C-labelled zymonic acid. *Nat Commun*. 2017;8:9, 15126.
21. Hundshammer C, Düwel S, Ruseckas D, et al. Hyperpolarized amino acid derivatives as multivalent magnetic resonance pH sensor molecules. *Sensors*. 2018;18(2):600-615.
22. Korenchan DE, Taglang C, von Morze C, et al. Dicarboxylic acids as pH sensors for hyperpolarized ¹³C magnetic resonance spectroscopic imaging. *Analyst*. 2017;142(9):1429-1433.
23. Jindal AK, Merritt ME, Suh EH, Malloy CR, Sherry AD, Kovács Z. Hyperpolarized ⁸⁹Y complexes as pH sensitive NMR probes. *J Am Chem Soc*. 2010; 132(6):1784-1785.
24. Nardi-Schreiber A, Gamliel A, Harris T, et al. Biochemical phosphates observed using hyperpolarized ³¹P in physiological aqueous solutions. *Nat Commun*. 2017;8(1):341.
25. Flavell RR, von Morze C, Blecha JE, et al. Application of Good's buffers to pH imaging using hyperpolarized ¹³C MRI. *Chem Commun*. 2015;51(74): 14119-14122.
26. Jiang W, Lumata L, Chen W, et al. Hyperpolarized ¹⁵N-pyridine derivatives as pH-sensitive MRI agents. *Sci Rep*. 2015;5:9104.
27. Shchepin RV, Barskiy DA, Coffey AM, et al. ¹⁵N hyperpolarization of imidazole-¹⁵N₂ for magnetic resonance pH sensing via SABRE-SHEATH. *ACS Sens*. 2016;1(6):640-644.
28. Ball DR, Rowlands B, Dodd MS, et al. Hyperpolarized butyrate: A metabolic probe of short chain fatty acid metabolism in the heart. *Magn Reson Med*. 2014;71(5):1663-1669.
29. Khemtong C, Carpenter NR, Lumata LL, et al. Hyperpolarized ¹³C NMR detects rapid drug-induced changes in cardiac metabolism. *Magn Reson Med*. 2015;74(2):312-319.
30. Mariotti E, Orton MR, Eerbeek O, et al. Modeling non-linear kinetics of hyperpolarized [1-¹³C] pyruvate in the crystalloid-perfused rat heart. *NMR Biomed*. 2016;29(4):377-386.
31. Moreno KX, Sabelhaus SM, Merritt ME, Sherry AD, Malloy CR. Competition of pyruvate with physiological substrates for oxidation by the heart: implications for studies with hyperpolarized [1-¹³C]pyruvate. *Am J Physiol-Heart Circul Physiol*. 2010;298(5):H1556-H1564.
32. Purmal C, Kucejova B, Sherry AD, Burgess SC, Malloy CR, Merritt ME. Propionate stimulates pyruvate oxidation in the presence of acetate. *Am J Physiol-Heart Circul Physiol*. 2014;307(8):H1134-H1141.

33. Schroeder MA, Atherton HJ, Ball DR, et al. Real-time assessment of Krebs cycle metabolism using hyperpolarized ^{13}C magnetic resonance spectroscopy. *FASEB J*. 2009;23(8):2529-2538.
34. Weiss K, Mariotti E, Hill DK, et al. Developing hyperpolarized ^{13}C spectroscopy and imaging for metabolic studies in the isolated perfused rat heart. *Appl Magn Reson*. 2012;43(1):275-288.
35. Merritt ME, Harrison C, Storey C, Sherry AD, Malloy CR. Inhibition of carbohydrate oxidation during the first minute of reperfusion after brief ischemia: NMR detection of hyperpolarized $^{13}\text{CO}_2$ and H^{13}CO_3 . *Magn Reson Med*. 2008;60(5):1029-1036.
36. Ball DR, Cruickshank R, Carr CA, et al. Metabolic imaging of acute and chronic infarction in the perfused rat heart using hyperpolarised $[1-^{13}\text{C}]$ pyruvate. *NMR Biomed*. 2013;26(11):1441-1450.
37. Atherton HJ, Dodd MS, Heather LC, et al. Role of PDH inhibition in the development of hypertrophy in the hyperthyroid rat heart: a combined magnetic resonance imaging and hyperpolarized magnetic resonance spectroscopy study. *Circulation*. 2011;123(22):2552-2561.
38. Dodd MS, Atherton HJ, Carr CA, et al. Impaired in vivo mitochondrial Krebs cycle activity after myocardial infarction assessed using hyperpolarized magnetic resonance spectroscopy. *Circ Cardiovasc Imaging*. 2014;7(6):895-904.
39. Dodd MS, Ball DR, Schroeder MA, et al. In vivo alterations in cardiac metabolism and function in the spontaneously hypertensive rat heart. *Cardiovasc Res*. 2012;95(1):69-76.
40. Schroeder MA, Lau AZ, Chen AP, et al. Hyperpolarized ^{13}C magnetic resonance reveals early- and late-onset changes to in vivo pyruvate metabolism in the failing heart. *Eur J Heart Fail*. 2013;15(2):130-140.
41. Lau AZ, Miller JJ, Robson MD, Tyler DJ. Simultaneous assessment of cardiac metabolism and perfusion using copolarized $[1-^{13}\text{C}]$ pyruvate and ^{13}C -urea. *Magn Reson Med*. 2017;77(1):151-158.
42. Lauritzen MH, Magnusson P, Laustsen C, et al. Imaging regional metabolic changes in the ischemic rat heart in vivo using hyperpolarized $[1-^{13}\text{C}]$ pyruvate. *Tomography*. 2017;3(3):123-130.
43. Lau AZ, Miller JJ, Tyler DJ. Mapping of intracellular pH in the in vivo rodent heart using hyperpolarized $[1-^{13}\text{C}]$ pyruvate. *Magn Reson Med*. 2017;77(5):1810-1817.
44. Miller JJ, Lau AZ, Teh I, et al. Robust and high resolution hyperpolarized metabolic imaging of the rat heart at 7 T with 3D spectral-spatial EPI. *Magn Reson Med*. 2016;75(4):1515-1524.
45. Schroeder MA, Cochlin LE, Heather LC, Clarke K, Radda GK, Tyler DJ. In vivo assessment of pyruvate dehydrogenase flux in the heart using hyperpolarized carbon-13 magnetic resonance. *Proc Natl Acad Sci U S A*. 2008;105(33):12051-12056.
46. Wespi P, Steinhäuser J, Kwiatkowski G, Kozerke S. High-resolution hyperpolarized metabolic imaging of the rat heart using k-t PCA and k-t SPARSE. *NMR Biomed*. 2018;31(2):e3876.
47. Weiss K, Sigfridsson A, Wissmann L, et al. Accelerating hyperpolarized metabolic imaging of the heart by exploiting spatiotemporal correlations. *NMR Biomed*. 2013;26(11):1380-1386.
48. Yoshihara HA, Bastiaansen JA, Berthonneche C, Comment A, Schwitler J. Assessing ischemic myocardial metabolism in vivo with hyperpolarized ^{13}C : relating the metabolic perturbation to the area at risk. *J Cardiovasc Magn Reson*. 2015;17(Suppl 1):O97.
49. Yoshihara HA, Bastiaansen JA, Berthonneche C, Comment A, Schwitler J. An intact small animal model of myocardial ischemia-reperfusion: Characterization of metabolic changes by hyperpolarized ^{13}C MR spectroscopy. *Am J Physiol-Heart Circul Physiol*. 2015;309(12):H2058-H2066.
50. Wespi P, Steinhäuser J, Kwiatkowski G, Kozerke S. Overestimation of cardiac lactate production caused by liver metabolism of hyperpolarized $[1-^{13}\text{C}]$ pyruvate. *Magn Reson Med*. 2018;80(5):1882-1890.
51. Dominguez-Viqueira W, Geraghty BJ, Lau JYC, Robb FJ, Chen AP, Cunningham CH. Intensity correction for multichannel hyperpolarized ^{13}C imaging of the heart. *Magn Reson Med*. 2016;75(2):859-865.
52. Lau AZ, Chen AP, Ghugre NR, et al. Rapid multislice imaging of hyperpolarized ^{13}C pyruvate and bicarbonate in the heart. *Magn Reson Med*. 2010;64(5):1323-1331.
53. Lau AZ, Chen AP, Barry J, et al. Reproducibility study for free-breathing measurements of pyruvate metabolism using hyperpolarized ^{13}C in the heart. *Magn Reson Med*. 2013;69(4):1063-1071.
54. Frijia F, Santarelli MF, Koellisch U, et al. 16-channel surface coil for ^{13}C -hyperpolarized spectroscopic imaging of cardiac metabolism in pig heart. *J Med Biol Eng*. 2016;36(1):53-61.
55. Månsson S, Petersson JS, Scheffler K. Fast metabolite mapping in the pig heart after injection of hyperpolarized ^{13}C -pyruvate with low-flip angle balanced steady-state free precession imaging. *Magn Reson Med*. 2012;68(6):1894-1899.
56. Tougaard RS, Hansen ESS, Laustsen C, et al. Acute hypertensive stress imaged by cardiac hyperpolarized $[1-^{13}\text{C}]$ pyruvate magnetic resonance. *Magn Reson Med*. 2018;80(5):2053-2061.
57. Lau AZ, Chen AP, Cunningham CH. Integrated Bloch-Siegert B1 mapping and multislice imaging of hyperpolarized ^{13}C pyruvate and bicarbonate in the heart. *Magn Reson Med*. 2012;67(1):62-71.
58. Golman K, Petersson JS, Magnusson P, et al. Cardiac metabolism measured noninvasively by hyperpolarized ^{13}C MRI. *Magn Reson Med*. 2008;59(5):1005-1013.
59. Cunningham CH, Lau JYC, Chen AP, et al. Hyperpolarized ^{13}C metabolic MRI of the human heart initial experience. *Circ Res*. 2016;119(11):1177-1182.
60. Rider OJ, Apps A, Miller JJJ, et al. Noninvasive in vivo assessment of cardiac metabolism in the healthy and diabetic human heart using hyperpolarized ^{13}C MRI. *Circ Res*. 2020;126(6):725-736.
61. Seymour AM, Giles L, Ball V, et al. In vivo assessment of cardiac metabolism and function in the abdominal aortic banding model of compensated cardiac hypertrophy. *Cardiovasc Res*. 2015;106(2):249-260.
62. Moon C-M, Kim Y-H, Ahn Y-K, Jeong M-H, Jeong G-W. Metabolic alterations in acute myocardial ischemia-reperfusion injury and necrosis using in vivo hyperpolarized $[1-^{13}\text{C}]$ pyruvate MR spectroscopy. *Sci Rep*. 2019;9(1):18427.
63. Harris T, Uppala S, Lev-Cohain N, et al. Hyperpolarized product selective saturating-excitations for determination of changes in metabolic reaction rates in real-time. *NMR Biomed*. 2020;33(2):e4189.
64. Kurhanewicz J, Vigneron DB, Ardenkjaer-Larsen JH, et al. Hyperpolarized ^{13}C MRI: Path to clinical translation in oncology. *Neoplasia*. 2019;21(1):1-16.

65. Miloushev VZ, Granlund KL, Boltyanskiy R, et al. Metabolic imaging of the human brain with hyperpolarized ^{13}C pyruvate demonstrates ^{13}C lactate production in brain tumor patients. *Cancer Res.* 2018;78(14):3755-3760.
66. Park I, Larson PE, Gordon JW, et al. Development of methods and feasibility of using hyperpolarized carbon-13 imaging data for evaluating brain metabolism in patient studies. *Magn Reson Med.* 2018;80(3):864-873.
67. Grist JT, McLean MA, Riemer F, et al. Quantifying normal human brain metabolism using hyperpolarized $[1-^{13}\text{C}]$ pyruvate and magnetic resonance imaging. *Neuroimage.* 2019;189:171-179.
68. Nelson SJ, Kurhanewicz J, Vigneron DB, et al. Metabolic imaging of patients with prostate cancer using hyperpolarized $[1-^{13}\text{C}]$ pyruvate. *Sci Transl Med.* 2013;5(198):198ra108.
69. Stødkilde-Jørgensen H, Laustsen C, Hansen ESS, et al. Pilot study experiences with hyperpolarized $[1-^{13}\text{C}]$ pyruvate MRI in pancreatic cancer patients. *J Magn Reson Imaging.* 2019;51(3):961-963.
70. Autry AW, Hashizume R, James CD, Larson PEZ, Vigneron DB, Park I. Measuring tumor metabolism in pediatric diffuse intrinsic pontine glioma using hyperpolarized carbon-13 MR metabolic imaging. *Contrast Media Mol Imaging.* 2018;2018:1-6, 3215658.
71. Chung BT, Chen H-Y, Gordon J, et al. First hyperpolarized $[2-^{13}\text{C}]$ pyruvate MR studies of human brain metabolism. *J Magn Reson.* 2019;309:106617.
72. Jian Z, Chen YJ, Shimkunas R, et al. In vivo cannulation methods for cardiomyocytes isolation from heart disease models. *PLoS One.* 2016;11(8):e0160605.
73. Sutherland FJ, Hearse DJ. The isolated blood and perfusion fluid perfused heart. *Pharmacol Res.* 2000;41(6):613-627.
74. Lateef R, Al-Masri A, Alyahya A. Langendorff's isolated perfused rat heart technique: A review. *Int J Basic Clin Pharmacol.* 2015;4:1314-1322.
75. Cross HR, Radda GK, Clarke K. The role of Na^+/K^+ ATPase activity during low-flow ischemia in preventing myocardial injury - A ^{31}P , ^{23}Na and ^{87}Rb NMR spectroscopic study. *Magn Reson Med.* 1995;34(5):673-685.
76. Cross HR, Clarke K, Opie LH, Radda GK. Is lactate-induced myocardial ischaemic injury mediated by decreased pH or increased intracellular lactate? *J Mol Cell Cardiol.* 1995;27(7):1369-1381.
77. Clarke K, Oconnor AJ, Willis RJ. Temporal relation between energy metabolism and myocardial function during ischemia and reperfusion. *Am J Physiol.* 1987;253(2):H412-H421.
78. Kolwicz SC, Tian R. Assessment of cardiac function and energetics in isolated mouse hearts using ^{31}P NMR spectroscopy. *J Vis Exp.* 2010;42:2069.
79. Nakadate Y, Sato H, Oguchi T, et al. Glycemia and the cardioprotective effects of insulin pre-conditioning in the isolated rat heart. *Cardiovasc Diabetol.* 2017;16(1):43.
80. Lauritzen MH, Laustsen C, Butt SA, et al. Enhancing the C-13 bicarbonate signal in cardiac hyperpolarized 1-C-13 pyruvate MRS studies by infusion of glucose, insulin and potassium. *NMR Biomed.* 2013;26(11):1496-1500.
81. Young AA, Barnes H, Davison D, Neubauer S, Schneider JE. Fast left ventricular mass and volume assessment in mice with three-dimensional guide-point modeling. *J Magn Reson Imaging.* 2009;30(3):514-520.
82. Adler-Levy Y, Nardi-Schreiber A, Harris T, et al. In-cell determination of lactate dehydrogenase activity in a luminal breast cancer model - ex vivo investigation of excised xenograft tumor slices using dDNP hyperpolarized $[1-^{13}\text{C}]$ pyruvate. *Sensors.* 2019;19(9):2089.
83. Harris T, Gamliel A, Sosna J, Gomori JM, Katz-Brull R. Impurities of $[1-^{13}\text{C}]$ pyruvic acid and a method to minimize their signals for hyperpolarized pyruvate metabolism studies. *Appl Magn Reson.* 2018;49(10):1085-1098.
84. Massiot D, Fayon F, Capron M, et al. Modelling one- and two-dimensional solid-state NMR spectra. *Magn Reson Chem.* 2002;40(1):70-76.
85. Sharoni R, Olivson A, Chandra M, et al. A ^{31}P NMR study of preconditioned isolated perfused rat heart exposed to intermittent ischemia. *Magn Reson Med.* 1996;36(1):66-71.
86. Kopp SJ, Daar AA, Prentice RC, Tow JP, Feliksik JM. ^{31}P NMR-studies of the intact perfused rat-heart - a novel analytical approach for determining functional metabolic correlates, temporal relationships, and intracellular actions of cardiotoxic chemicals nondestructively in an intact organ model. *Toxicol Appl Pharmacol.* 1986;82(2):200-210.
87. Lutz NW, Le Fur Y, Chiche J, Pouyssegur J, Cozzone PJ. Quantitative in vivo characterization of intracellular and extracellular pH profiles in heterogeneous tumors: A novel method enabling multiparametric pH analysis. *Cancer Res.* 2013;73:4616.
88. Bailey IA, Williams SR, Radda GK, Gadian DG. Activity of phosphorylase in total global ischaemia in the rat heart. A phosphorus-31 nuclear-magnetic-resonance study. *Biochem J.* 1981;196(1):171-178.
89. Garlick PB, Radda GK, Seeley PJ. Studies of acidosis in the ischaemic heart by phosphorus nuclear magnetic resonance. *Biochem J.* 1979;184(3):547-554.
90. Yabe T, Mitsunami K, Inubushi T, Kinoshita M. Quantitative measurements of cardiac phosphorus metabolites in coronary artery disease by ^{31}P magnetic resonance spectroscopy. *Circulation.* 1995;92(1):15-23.
91. Steenbergen C, Deleew G, Rich T, Williamson JR. Effects of acidosis and ischemia on contractility and intracellular pH of rat-heart. *Circ Res.* 1977;41(6):849-858.
92. Garlick PB, Radda GK, Seeley PJ. Studies of acidosis in the ischemic heart by phosphorus nuclear magnetic-resonance. *Biochem J.* 1979;184(3):547-554.
93. Schroeder MA, Atherton HJ, Cochlin LE, Clarke K, Radda GK, Tyler DJ. The effect of hyperpolarized tracer concentration on myocardial uptake and metabolism. *Magn Reson Med.* 2009;61(5):1007-1014.
94. Lee HB, Blaufox MD. Blood-volume in the rat. *J Nucl Med.* 1985;26(1):72-76.
95. Sandhu GS, Asimakis GK. Mechanism of loss of adenine-nucleotides from mitochondria during myocardial-ischemia. *J Mol Cell Cardiol.* 1991;23(12):1423-1435.
96. Wengrowski AM, Kuzmiak-Glancy S, Jaimes R, Kay MW. NADH changes during hypoxia, ischemia, and increased work differ between isolated heart preparations. *Am J Physiol-Heart Circul Physiol.* 2014;306(4):H529-H537.
97. Opie LH. Myocardial-ischemia - metabolic pathways and implications of increased glycolysis. *Cardiovasc Drugs Ther.* 1990;4:777-790.
98. HMDB. L-Lactic acid. 2018; <http://www.hmdb.ca/metabolites/HMDB0000190>. Accessed 23 January 2020.
99. Katsura K, Asplund B, Ekholm A, Siesjo BK. Extracellular and intracellular pH in the brain during ischemia, related to tissue lactate content in normocapnic and hypercapnic rats. *Eur J Neurosci.* 1992;4(2):166-176.

100. Jokivarsi KT, Grohn HI, Grohn OH, Kauppinen RA. Proton transfer ratio, lactate, and intracellular pH in acute cerebral ischemia. *Magn Reson Med*. 2007;57(4):647-653.
101. Vesell ES, Fritz PJ, White EL. Effects of buffer pH ionic strength and temperature on lactate dehydrogenase isozymes. *Biochim Biophys Acta*. 1968;159(2):236-243.
102. Pearce FJ, Walajtysrode E, Williamson JR. Effects of work and acidosis on pyruvate-dehydrogenase activity in perfused rat hearts. *J Mol Cell Cardiol*. 1980;12(5):499-510.
103. Pawelczyk T, Easom RA, Olson MS. Effect of ionic strength and pH on the activity of pyruvate dehydrogenase complex from pig kidney cortex. *Arch Biochem Biophys*. 1992;294(1):44-49.
104. Bahrami N, Swisher CL, Von Morze C, Vigneron DB, Larson PEZ. Kinetic and perfusion modeling of hyperpolarized ^{13}C pyruvate and urea in cancer with arbitrary RF flip angles. *Quant Imaging Med Surg*. 2014;4(1):24-32.

SUPPORTING INFORMATION

Additional supporting information may be found online in the Supporting Information section at the end of this article.

How to cite this article: Shaul D, Azar A, Sapir G, et al. Correlation between lactate dehydrogenase/pyruvate dehydrogenase activities ratio and tissue pH in the perfused mouse heart: A potential noninvasive indicator of cardiac pH provided by hyperpolarized magnetic resonance. *NMR in Biomedicine*. 2021;34:e4444. <https://doi.org/10.1002/nbm.4444>